Symbiosis

www.symbiosisonline.org
www.symbiosisonlinepublishing.com

Research Article | SOJ Materials Science & Engineering | Open Access

Piezoelectric Characterization with Mechanical Excitation in PZT Bar with Non-Electrode Boundary Condition–k_{31} Mode Case

Maryam Majzoubi[1], Yuxuan Zhang[1*], Eberhard Hennig[2], Timo Scholehwar[2] and Kenji Uchino[1]

[1]International Center for Actuators and Transducers, The Pennsylvania State University, State College, PA, 16802, USA

[2]R&D Department, PI Ceramic GmbH, Lindenstrasse, 07589 Lederhose, Germany

Received: March 07, 2018; Accepted: March 23, 2018; Published: April 10, 2018

***Corresponding author:** Yuxuan Zhang, International Center for Actuators and Transducers, The Pennsylvania State University, 141 Energy and Environment Laboratory, State College, PA, 16801, USA, Tel:+814-699-0400; E-mail: yuz381@psu.edu*

Abstract

We introduced an advanced piezoelectric characterization method with mechanical excitation on partial electrode samples, which can determine additional physical parameters the conventional full-electrode electrical excitation method cannot provide. A non-electrode sample with only 10% electrode at the center of a rectangular k_{31} piezoelectric plate has the benefits for measuring the extensive parameters directly and much precisely. In this paper, we derived first the exact analytical solutions on the partial electrode configuration, including the 10% mechanical excitation part in a partial non-electrode sample for calculating there sonance vibration mode and mechanical quality factors of the composite bar sample for obtaining the extensive elastic compliance and loss factor. The result suggests that the almost accurate values can be obtained even for a specimen with up to 40% center electrode area in the k_{31} mode samples. Second objective is to compare three different simulations (ATILA FEM, 6-terminal Equivalent Circuit and Analytical Solution). This mechanical excitation method has the benefit in measuring physical parameters which cannot be obtained directly from the IEEE Standard electrical excitation method.

Keywords: Direct loss measurement; intensive and extensive parameters; resonance vibration mode; PZT; mechanical quality factor;

Introduction

Miniaturized piezoelectric devices have been replacing electromagnetic (EM) technologies such as motors and transformers, since the same size of devices could generate 10 times higher power density in miniaturized transducer areas [1-9]. The limitation of power in EM devices is mainly caused by the heat generation due to the ohmic losses (i.e., Joule heat) in the coils, dramatically increasing with reducing the lead wire diameter [10]. On the other hand, further miniaturization of piezoelectric devices is also restricted by heat generation due to inherent hysteresis losses, primarily originated from microscopic domain dynamics [11-14]. Therefore, it is necessary to study these losses as a function of input electric power under different boundary conditions.

There are three types of losses in piezoelectric materials; namely, elastic $tan\phi$, dielectric ($tan\delta$), and piezoelectric losses ($tan\theta$), which are respectively described as complex numbers in the elastic compliance, permittivity, and piezoelectric constant in the Equations (1-6) below [15,16]. Furthermore, each of these is classified into two kinds of 'intensive' and 'extensive' parameters [14,17]. Intensive parameters (externally controllable, electric field E, stress T), unlike the extensive ones (internally determined in a crystal, electric displacement D, strain S), do not depend on the size or volume of the material theoretically, since they are the ratio of two extensive properties [18,19]. The prime and non-prime loss parameters in Equations (1-6) correspond to the intensive and extensive losses, respectively.

$$s^{E*} = s^{E}(1 - j\tan\varphi') \quad (1) \qquad c^{D*} = c^{D}(1 + j\tan\varphi) \quad (2)$$

$$\varepsilon^{T*} = \varepsilon^{T}(1 - j\tan\delta') \quad (3) \qquad \beta^{S*} = \beta^{S}(1 + j\tan\delta) \quad (4)$$

$$d^{*} = d(1 - j\tan\theta') \quad (5) \qquad h^{*} = h(1 + j\tan\theta) \quad (6)$$

s^E is the elastic compliance under constant electric field, and ε^T is the dielectric constant under constant stress; while c^D is the elastic stiffness under constant electric displacement (open circuit), and β^S is the inverse dielectric constant under constant strain (mechanically clamped condition). It should be noted that intensive losses, generally, exhibit larger values than the extensive ones [20,21]. Moreover, d is the piezoelectric constant, and h is the inverse piezoelectric charge constant. In order to have the numerically-positive loss tangents, consistent with the experimental measurements, the sign of the imaginary part for the intensive and extensive losses are considered to be negative and positive accordingly [14,20,22].

Mechanical quality factor Q_m is a sort of figure of merit for heat generation and device efficiency [23,24]; the larger Q_m, the better in efficiency. It can be calculated both for the resonance (Q_A, A-type resonance), and anti-resonance (Q_B, B-type resonance)

frequencies, from the 3dB bandwidth method in the admittance or impedance curve. The maximum and minimum points in the admittance curve attribute to the resonance (f_a) and anti-resonance (f_b) frequencies roughly. And the 3dB bandwidth is the distance between the points having the frequencies $1/\sqrt{2}$ (or $\sqrt{2}$) times the resonance (or anti-resonance) point in the admittance spectrum. The mechanical quality factor is then defined as follows, in which $(f_{a1} - f_{a2})$ or $(f_{b1} - f_{b2})$ attributes to the 3dB down/up full-bandwidths [22]:

$$Q_A = \frac{f_a}{f_{a1} - f_{a2}} (7)$$

$$Q_B = \frac{f_b}{f_{b1} - f_{b2}} (8)$$

In the conventional methods of measuring the properties of piezoelectric materials in the k_{31} fundamental mode with a full electrode configuration, only the intensive parameters can be measured directly, and the extensive ones are derived indirectly through the coupling factor, defined in Equation 10 as follows:

$$s_{11}^D = s_{11}^E \left(1 - k_{31}^2\right) (9)$$

$$k_{31}^2 = \frac{d_{31}^2}{s_{11}^E \varepsilon_{33}^T} \quad (10)$$

Furthermore, the same argument is true for the loss calculation through the "K matrix", which is involutory, exhibiting a full symmetry relationship between the intensive and extensive losses (i.e., $K^2 = I$, or $K = K^{-1}$) [21].

$$\begin{bmatrix} tan\delta \\ tan\phi \\ tan\theta \end{bmatrix} = K \begin{bmatrix} tan\delta' \\ tan\phi' \\ tan\theta' \end{bmatrix}, K = \frac{1}{1 - k_{31}^2} \begin{bmatrix} 1 & k_{31}^2 & -2k_{31}^2 \\ k_{31}^2 & 1 & -2k_{31}^2 \\ 1 & 1 & -1 - k_{31}^2 \end{bmatrix}, (11)$$

The intensive dielectric loss can be calculated with a capacitance meter at an off-resonance frequency. According to our recent research, the dielectric constant and loss determined at an off-resonance frequency are almost the same as determined at the resonance frequency under small vibration level [29]. Using the conventional IEEE Standard k_{31} type sample with a full electrode configuration, we could determine only the intensive parameters and loss factors. The intensive mechanical loss is the inverse of mechanical quality factor Q_A at the k_{31} resonance mode (Equation 12), and then the intensive piezoelectric loss can be derived from these two losses and the mechanical quality factor Q_B at the anti-resonance frequencies as in Equation 13 [21]:

$$tan\phi_{11}' = \frac{1}{Q_{A,31}} (12)$$

$$tan\theta_{31}' = \frac{1}{2}\left(tan\delta_{33}' + tan\phi_{11}'\right) + \frac{1}{4}\left(\frac{1}{Q_{A,31}} - \frac{1}{Q_{B,31}}\right)\left(1 + \left(\frac{1}{k_{31}} - k_{31}\right)^2 \Omega_{b,31}^2\right) (13)$$

Here $\Omega_{b,31}$ is the normalized angular frequency of the antiresonance given by $\Omega_{b,31} = \frac{\omega_b l}{2v_{11}^E}$. Then the extensive (non-prime) losses could be derived indirectly from the "K" matrix (Equation 11).

However, since the dielectric loss measurement cannot be very precise, in comparison with the mechanical loss, the error propagation in the extensive loss calculation from the "K" matrix is quite high, resulting in large uncertainty in extensive loss values [20]. We would like to emphasize again that the precise determination of both intensive & extensive losses is essential to improve the simulation accuracy of high power density piezoelectric devices, which is the motivation of our new method by using a partial electrode configuration.

Our research target is to establish the mechanical excitation method for characterizing piezoelectric properties for supplementing the conventional electrical excitation methods. (Figure 1) illustrates vibration modes of k31 type piezoelectric plates: resonance, antiresonance modes of the electroded plate, and resonance mode of the non-electroded plate under electric field (top) and mechanical excitation (bottom). In the conventional full-electrode case under electrical excitation, the maximum and minimum admittance frequencies correspond to the piezoelectric resonance and antiresonance frequencies roughly. The same frequencies are obtained as the mechanical resonance frequencies under mechanical excitation, with short- and open-circuit conditions of top and bottom electrodes. However, without electrodes, the resonance cannot be monitored under electrical excitation method, while this resonance can be measured with the mechanical excitation method, which can provide the information on D-constant parameters, such as s_{11}^D and sound velocity v^D.

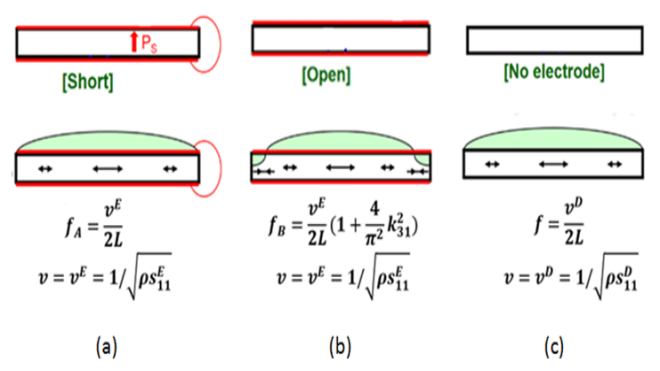

Figure 1: Equivalent electrode configuration and vibration modes of k31 type piezoelectric plates: **(a)** resonance, **(b)** anti resonance modes under electrical excitation, and **(c)** resonance mode under mechanical excitation.

An advanced method of measuring the extensive (i.e., D constant) elastic compliance and mechanical loss directly in the k_{31} mode has been proposed in our recent work by using non-electrode samples which have only 10% electrodes at the middle of the top and bottom surfaces, as shown in (Figure 2d) [25].The center electrode part acts similarly as an actuator to mechanically

excite the vibration in the whole sample (including the non-electrode parts), and simultaneously monitoring the responding signal. The non-electrode parts are the loads with the extensive boundary condition (D constant, rather than E constant on the electrode). The properties of the load material can be monitored through the admittance/impedance spectrum of the small center actuator part. The comparison between conventional IEEE standard k_{31} mode piezoelectric measurement and our novel partial electrode measurement method is illustrated in (Table1). By using our advanced partial electrode mechanical excitation method, both intensive and extensive parameters can be measured without further derivation.

Table 1: Comparison between IEEE Standard electrical excitation method and partial electrode mechanical excitation method

Excitation Method	Name	Electrode Configuration	Features
Electrical Excitation	IEEE Standard	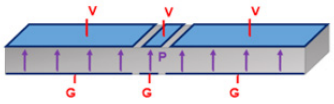	Only Intensive (constant E condition) parameters can be measured
Mechanical Excitation	Partial Electrode-Short Circuit Mode	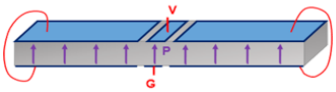	Corresponds to resonance mode of IEEE standard
	Partial Electrode-Open Circuit Mode	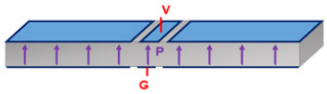	Corresponds to antiresonance mode of IEEE standard
	Non-Electrode Mode	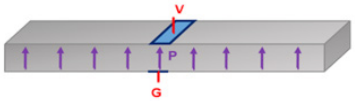	Directly Measure Extensive (constant D condition)

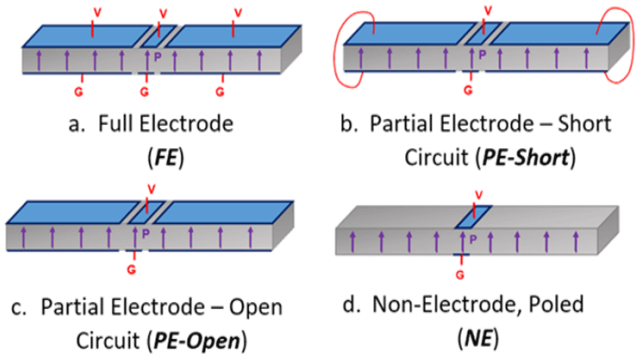

Figure 2: Schematic view of (a) full-electrode (FE), (b) partial electrode – short-circuit, (c) partial electrode – open circuit, and (d) non-electrode (NE) samples.

The partial electrode samples with electrode load (short- and open-circuit) were also prepared and measured as reference data. The schematic view of (a) full-electrode (FE), (b) partial electrode – short-circuit, (c) partial electrode – open circuit, and (d) non-electrode (NE) samples are shown in (Figure 2). The preliminary results were examined by neglecting the 10% actuator part difference and reported in [25]. This paper present sa precise analysis on the elastic compliance (or resonance frequency) and its corresponding loss (mechanical loss)in this PZT composite bar with both intensive (electrode) and extensive (non-electrode) boundary conditions, and to verify the feasibility of this methodology to more general sample geometry applications.

The admittance spectra of the full electrode and three partial electrode samples were measured as shown in (Figure 3). The full-electrode (FE) sample corresponds to a conventional rectangular k_{31} mode sample. PE-Short attributes to the pure E-constant condition, namely the resonance mode. As demonstrated in (Figure 3), the resonance frequency of this sample is almost the same as the FE one, and its anti-resonance frequency occurs at a much lower frequency. This is because the electrode area for actuator part in the PE-Short sample covers only 10% of the total length, and the load parts are still short circuit during the anti-resonance frequency. Therefore, its anti-resonance frequency happens between the resonance and anti-resonance frequencies of FE sample. On the contrary, the anti-resonance frequency of the PE-Open sample is the same as the one of the FE sample, and its resonance frequency occurs in much higher frequency,

because only the center part is excited and the outside parts are just mechanical loads with an open circuit, leading to apparently a lower electromechanical coupling factor. This case corresponds to the anti-resonance mode. Since we consider the k_{31} mode and also there is no electric field on the surface along the length direction (i.e., X-axis), the mechanical resonance of the PE-Open happens between the pure E (i.e., PE-Short) and D constant (i.e., NE) conditions.

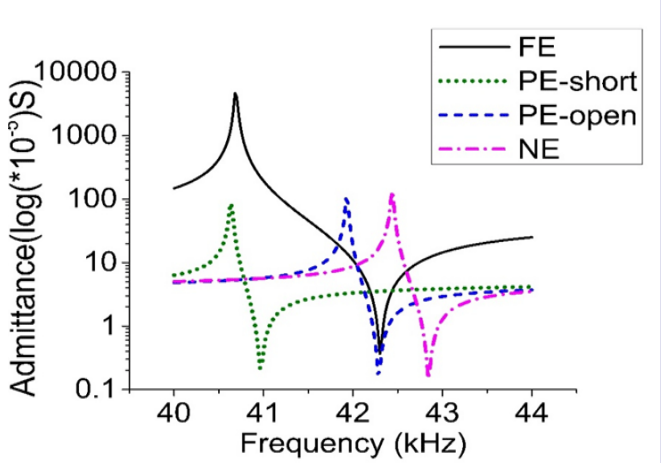

Figure 3: Experimental Results - Admittance spectrum of the full and partial electrode samples.

It is notable that the NE piezoelectric behaves the D-constant performance (except for a small electrode portion for excitation, which we neglected from the analysis in the previous paper [25]). Its losses would also mostly attribute to the extensive ones, which we could measure directly as the first trial. Since the elastic compliance under extensive condition (D-constant) is lower than the intensive one (E-constant), which means having a larger stiffness, higher resonance and anti-resonance frequencies are observed, in comparison to the FE sample and also the other partial electrode samples. It is noteworthy again that the resonance measurement on the non-electrode sample is possible only by using the mechanical excitation method.

In this paper, we describe first an accurate linear analytic solution in a continuum media, which is simple to use for calculating the resonance vibration mode and mechanical quality factors in a non-electrode sample. This is achieved by solving constitutive and dynamic equations in a composite bar by applying different boundary conditions, for the actuator and load parts with various electrode areas. Second objective is to compare three different simulations (ATILA FEM, 6-terminal Equivalent Circuit and Analytical Solution).

Theoretical Derivation

When the length L, width w and thickness b satisfy L >> w >> b in a rectangular shape piezoelectric specimen, the two basic constitutive equations in k31 mode piezoelectric materials are as follows in a linear first-approximation [28],

$$x_1 = s_{11}^E T_1 + d_{31} E_3 \quad (14)$$

$$D_3 = \varepsilon_0 \varepsilon_{33}^T E_3 + d_{31} T_1 \quad (15)$$

The x_1 and T_1 are strain and stress in direction 1 (longitude L), perpendicular to the poling direction. E_3 And D_3 is the electric field and dielectric displacement in the polling direction 3 (thickness b). The s_{11}^E is the elastic compliance for both stress and strain in direction 1 under the constant applied electric field. The $\varepsilon_0 \varepsilon_{33}^T$ is the permittivity for electric field and dielectric displacement in direction 3 under constant external stress. By assuming the stress to be zero in directions apart from the longitudinal vibration one in a long thin plate (L >> w >> b, k_{31} mode), the dynamic equation for extensional vibration is given as in Equation 16, in which u and x are the displacement and position in direction 1, and is the material's density[17],

$$\rho \frac{\partial^2 u}{\partial t^2} = F = \frac{\partial T_1}{\partial x} \quad (16)$$

By introducing the constitutive equations in the above equation, and allowing $x_1 = \frac{\partial u}{\partial x}$, two different cases of boundary conditions, electrode and non-electrode ones, are considered. Refer to (Figure 4). We introduce a parameter '*a*' to represent the electrode coverage rate on the plate specimen (a = 1 corresponds to a full electrode configuration). Firstly, taking into account that $\left(\frac{\partial E_3}{\partial x}\right) = 0$ for the electrode part due to the equal potential of each electrode, the following harmonic vibration equation is derived,

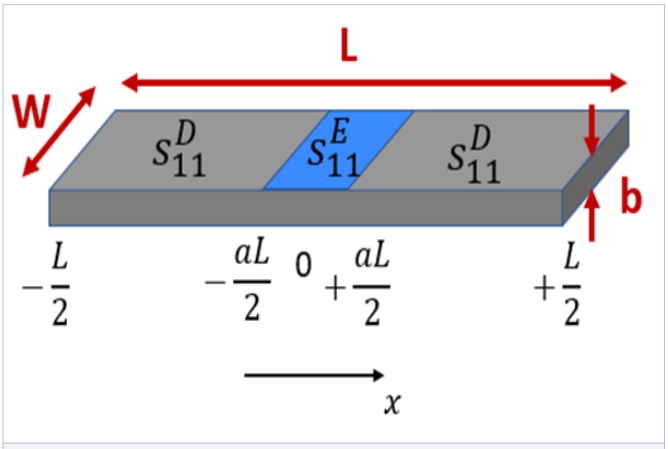

Figure 4: Non-electrode sample with 'a' fraction electrode at the center.

$$-\omega^2 \rho s_{11}^E u(x) = \frac{\partial^2 u(x)}{\partial x^2} \quad (17)$$

By substituting the general standing-wave form of the displacement equation as $u = u(x) e^{j\omega t}$, the following solution for the displacement of the electrode part can be obtained, since $u_e(x)$ should be equal to zero at x = 0 (center of gravity):

$$u_e(x) = A_e \sin\left(\frac{\omega}{v^E} x\right) \quad (18)$$

Secondly, by allowing $\left(\frac{\partial D_3}{\partial x}\right) = 0$ for the non-electrode area, the harmonic vibration equation and final solution can be derived as (for $|x| > aL/2$), in which the displacement equation with

positive sign for B_n correspond to the positive position x.

$$-\omega^2 \rho s_{11}^E (1-k_{31}^2) u(x) = \frac{\partial^2 u(x)}{\partial x^2} \quad (19)$$

$$u_n(x) = A_n \sin\left(\frac{\omega}{v^D} x\right) \pm B_n \cos\left(\frac{\omega}{v^D} x\right) \quad (20)$$

The $v^E = \frac{1}{\sqrt{\rho s_{11}^E}}$, and $v^D = \frac{1}{\sqrt{\rho s_{11}^D}}$ in these equations are the sound velocities for the above two conditions. Here, and for the rest of this paper, subscript 'e' or 'n' denotes the electrode or non-electrode parameters.

Therefore, the strain and stress for the electrode and non-electrode parts can be inferred as:

$$x_{1e}(x) = \frac{\partial u_e}{\partial x} = A_e \frac{\omega}{v^E} \cos\left(\frac{\omega}{v^E} x\right) \quad (21)$$

$$x_{1n}(x) = \frac{\partial u_n}{\partial x} = A_n \frac{\omega}{v^D} \cos\left(\frac{\omega}{v^D} x\right) - B_n \frac{\omega}{v^D} \sin\left(\frac{\omega}{v^D} x\right) \quad (22)$$

$$T_{1e}(x) = \frac{x_{1e}}{s_{11}^E} - \left(\frac{d_{31}}{s_{11}^E}\right) E_{3e} \quad (23)$$

$$T_{1n}(x) = \frac{x_{1n}}{s_{11}^E} - \left(\frac{d_{31}}{s_{11}^E}\right) E_{3n}(x) \quad (24)$$

E_{3e}, the electric field of the electrode area, is a constant value with respect to position which is known and can be calculated from the applied voltage to the sample. D_{3n} is also a constant value, since the non-electrode part cannot provide free charge, therefore $\nabla D = \rho = 0$. Furthermore, from $D = \varepsilon_0 E + P$ and the fact that for no electrode condition depolarization field E is proportion to the negative polarization (-P), therefore, $D_{3n} = 0$, and by giving $E_{3n}(x) = -\frac{d_{31}}{\varepsilon_0 \varepsilon_{33}^X} T_{1n}(x) + \frac{D_{3n}}{\varepsilon_0 \varepsilon_{33}^X} == -\frac{d_{31}}{\varepsilon_0 \varepsilon_{33}^X} T_{1n}(x)$ we have,

$$T_{1n}(x) = \frac{x_{1n}}{s_{11}^E (1-k_{31}^2)} = \frac{x_{1n}}{s_{11}^D} \quad (25)$$

There are three unknown parameters in the above equations, namely: A_e, A_n, and B_n, which can be solved by introducing three boundary conditions as follows:

1. Continuation of displacement at $x = \pm\frac{aL}{2}$ (the interface of electrode and non-electrode parts). The strain can exhibit discontinuity at $x = \pm\frac{aL}{2}$

2. Continuation of stress at $x = \pm\frac{aL}{2}$

3. Stress being zero at the plate end $x = \pm\frac{L}{2}$

The parameter "a" was introduced to describe the electrode coverage rate (0 < a < 1). These can be summarized in the following matrix relationship, and the solution for unknown parameters are given in Equation (27-29),

$$\begin{bmatrix} \sin\left(\frac{\omega}{v^E}\frac{aL}{2}\right) & -\sin\left(\frac{\omega}{v^D}\frac{aL}{2}\right) & -\cos\left(\frac{\omega}{v^D}x\frac{aL}{2}\right) \\ \frac{\omega}{v^E}\cos\left(\frac{\omega}{v^E}\frac{aL}{2}\right) & -\frac{\omega}{v^D}\frac{1}{1-k_{31}^2}\cos\left(\frac{\omega}{v^D}\frac{aL}{2}\right) & \frac{\omega}{v^D}\frac{1}{1-k_{31}^2}\sin\left(\frac{\omega}{v^D}\frac{aL}{2}\right) \\ 0 & \frac{\omega}{v^D}\frac{1}{1-k_{31}^2}\cos\left(\frac{\omega}{v^D}\frac{L}{2}\right) & -\frac{\omega}{v^D}\frac{1}{1-k_{31}^2}\sin\left(\frac{\omega}{v^D}\frac{L}{2}\right) \end{bmatrix} \begin{bmatrix} A_e \\ A_n \\ B_n \end{bmatrix} = \begin{bmatrix} 0 \\ d_{31}E_{3e} \\ 0 \end{bmatrix} \quad (26)$$

$$A_n = \frac{d_{31}E_{3e}\sin\left(\frac{\omega}{v^E}\frac{aL}{2}\right)\sin\left(\frac{\omega}{v^D}\frac{L}{2}\right)}{\frac{\omega}{v^E}\cos\left(\frac{\omega}{v^D}\frac{(1-a)L}{2}\right)\cos\left(\frac{\omega}{v^E}\frac{aL}{2}\right) - \frac{\omega}{v^D(1-k_{31}^2)}\sin\left(\frac{\omega}{v^D}\frac{(1-a)L}{2}\right)\sin\left(\frac{\omega}{v^E}\frac{aL}{2}\right)} \quad (27)$$

$$B_n = \frac{d_{31}E_{3e}\sin\left(\frac{\omega}{v^E}\frac{aL}{2}\right)\cos\left(\frac{\omega}{v^D}\frac{L}{2}\right)}{\frac{\omega}{v^E}\cos\left(\frac{\omega}{v^D}\frac{(1-a)L}{2}\right)\cos\left(\frac{\omega}{v^E}\frac{aL}{2}\right) - \frac{\omega}{v^D(1-k_{31}^2)}\sin\left(\frac{\omega}{v^D}\frac{(1-a)L}{2}\right)\sin\left(\frac{\omega}{v^E}\frac{aL}{2}\right)} \quad (28)$$

$$A_e = \frac{d_{31}E_{3e}\cos\left(\frac{\omega}{v^D}\frac{(1-a)L}{2}\right)}{\frac{\omega}{v^E}\cos\left(\frac{\omega}{v^E}\frac{aL}{2}\right)\cos\left(\frac{\omega}{v^D}\frac{(1-a)L}{2}\right) - \frac{\omega}{v^D(1-k_{31}^2)}\sin\left(\frac{\omega}{v^E}\frac{aL}{2}\right)\sin\left(\frac{\omega}{v^D}\frac{(1-a)L}{2}\right)} \quad (29)$$

In order to derive the admittance equation, the current of the electrode (only on the center electrode part) is required which can be calculated from,

$$I = j\omega\iint D_{3e}\,dxdy = 2j\omega W\{\int_0^{\frac{aL}{2}} D_{3e}\,dx\} = 2j\omega W\{\int_0^{\frac{aL}{2}} (d_{31}(\frac{1}{s_{11}^E}A_e\frac{\omega}{v^E}\cos\left(\frac{\omega}{v^E}x\right) - \left(\frac{d_{31}}{s_{11}^E}\right)E_{3e}) + \varepsilon_0\varepsilon_{33}^T E_{3e})dx\} = 2j\omega W\left(\frac{d_{31}A_e}{s_{11}^E}\sin\left(\frac{\omega}{v^E}\frac{aL}{2}\right) + \varepsilon_0\varepsilon_{33}^T(1-k_{31}^2)E_{3e}\frac{aL}{2}\right) \quad (30)$$

Then, by defining the $E_{3e} = -\frac{V}{b}$ and $Y = -\frac{I}{V}$, and considering the losses and complex values as in Equation (1-6), the admittance equation is deduced:

$$Y = 2jW\frac{d_{31}^*}{bs_{11}^{E*}}\frac{d_{31}^*\cos\left(\frac{\omega}{v^{D*}}\frac{(1-a)L}{2}\right)}{\frac{1}{v^{E*}}\cos\left(\frac{\omega}{v^{E*}}\frac{aL}{2}\right)\cos\left(\frac{\omega}{v^{D*}}\frac{(1-a)L}{2}\right) - \frac{1}{v^{D*}(1-k_{31}^{*2})}\sin\left(\frac{\omega}{v^{E*}}\frac{aL}{2}\right)\sin\left(\frac{\omega}{v^{D*}}\frac{(1-a)L}{2}\right)} \sin\left(\frac{\omega}{v^{E*}}\frac{aL}{2}\right) + j\omega\varepsilon_0\varepsilon_{33}^{T*}(1-k_{31}^{*2})\frac{aLW}{b} \quad (31)$$

Note that we introduced '*' for the dielectric, elastic and piezoelectric parameters in order to introduce three losses to calculate the admittance curves accurately. v^{E*}, v^{D*}, and k_{31}* were calculated by putting these complex parameters in their corresponding equations, i.e. $v^E = \frac{1}{\sqrt{\rho s_{11}^{E*}}}$, $v^D = \frac{1}{\sqrt{\rho s_{11}^{D*}}}$, and $k_{31}^{*2} = \frac{d_{31}^{*2}}{s_{11}^{E*}\varepsilon_{33}^{T*}}$

Experimental and Analytical Results and Discussions

The non-electrode samples were made from the commercial 'hard' bulk PZT rectangular plates, PIC144 [PI Ceramic GmbH, Lederhose, Germany] with 40 x 5 x 1 mm^3, and the essential material properties as listed in the (Table 2), which were further used for analytical simulation. The permittivity and its dielectric loss were measured with an LCR meter at 100Hz frequency [SR715, Stanford Research Systems, Inc., Sunnyvale, CA]. The other parameters were derived directly or indirectly from the admittance spectrum, measured with the Precision Impedance Analyzer [4294A, Agilent Technologies, Santa Clara, CA] [25]. The picture of the full-electrode and non-electrode samples are shown in (Figure 5)

The admittance spectra for the different fractions of the center electrode ('*a*' values) can be calculated from the Equation 31, and shown in (Figure 6). For instance, *a* = 1 is the typical FE

Table 2: PIC144 piezoelectric ceramic material properties

Properties	Real Parameter	Intensive Loss (prime)	Extensive Loss (non-prime)
Dielectric	$\varepsilon_{33}^{T}/\varepsilon_0 = 1073$	$\tan\delta_{33}^{'} = 2.3\times10^{-3}$	$\tan\delta_{33} = 2.1\times10^{-3}$
Elastic	$s_{11}^{E} = 11.7\times10^{-12}\left[m^2/N\right]$	$tan\phi_{11}^{'} = 7.19\times10^{-4}$	$tan\phi_{11} = 5.8x10^{-4}$
Piezoelectric	$d_{31} = -103\times10^{-12}\left[C/N\right]$	$\tan\theta_{31}^{'} = 2.2\times10^{-3}$	$\tan\theta_{31} = 6.6\times10^{-4}$
Density	$\rho = 8080\left[kg/m^3\right]$	-	-

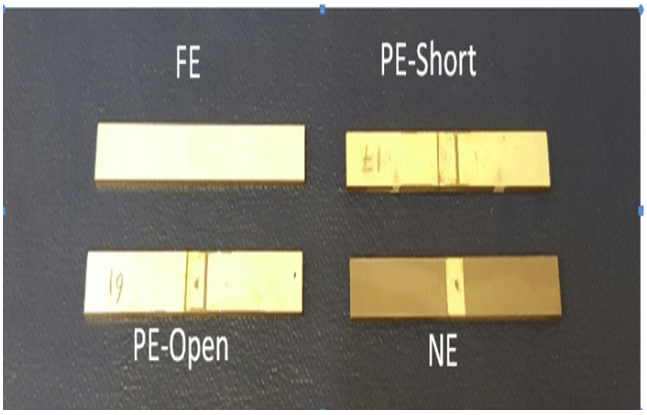

Figure 5: (a) full-electrode (FE), **(b)** partial electrode – short-circuit, **(c)** partial electrode – open circuit, and **(d)** non-electrode (NE) samples (a = 0.1).

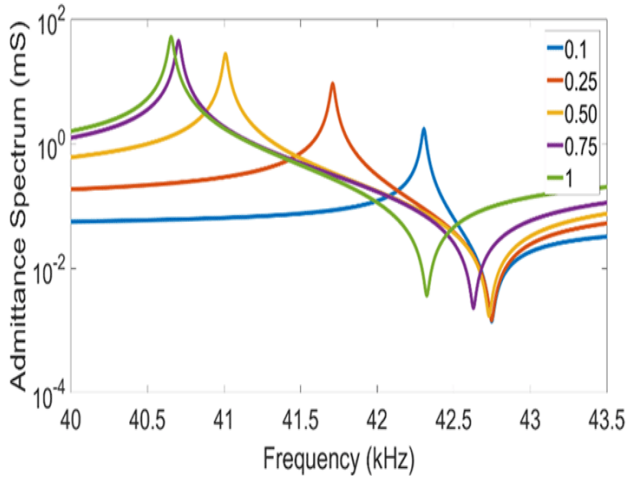

Figure 6: Admittance spectra for different fractions of the middle.

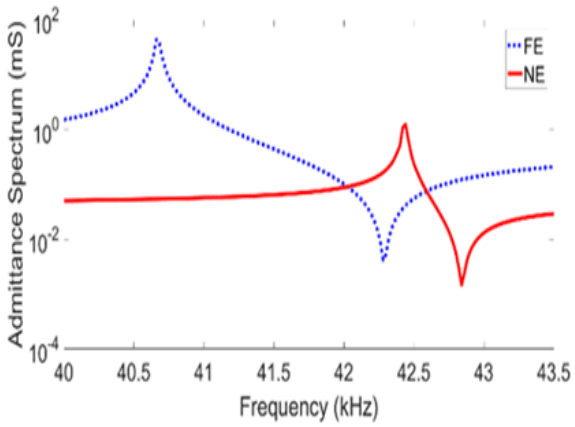

a. Experimental results - Admittance spectra

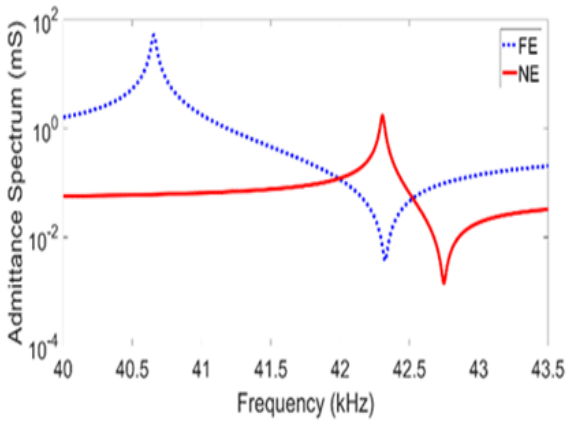

b. Analytical solution - Admittance spectrum

Figure 7: Experimental results and analytical solution admittance spectra comparison for FE and NE samples.

sample, and a = 0.1 is the partial NE one with 10% electrode in the middle.

(Figure 7) demonstrates the comparison between the analytical solution (b) and experimental results (a) admittance spectra, which verifies a good agreement in terms of the resonance frequencies and admittance values.

(Figure 8) illustrates the effect of the actuator portion '*a*' on the resonance frequencies and mechanical quality factors obtained from the 3dB bandwidth method of the admittance spectrum.

As demonstrated in (Figure 7,8), the resonance frequency fa (maximum peak in admittance curve), and Q_A value shift to lower monotonically with increasing the electrode portion. However, it is worth to note that the anti-resonance frequency f_b (minimum peak in admittance curve) and Q_B value do not change

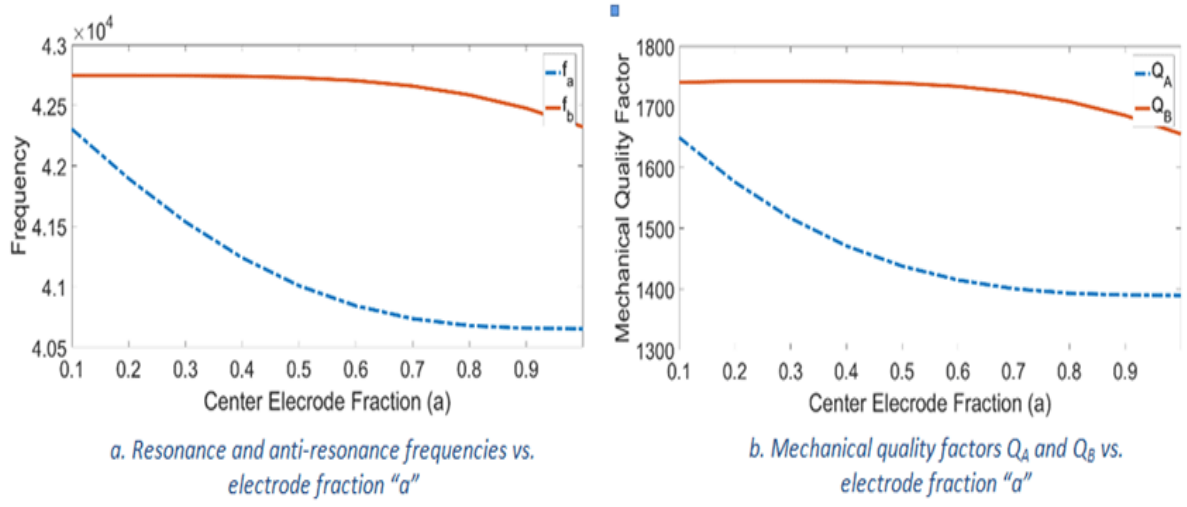

Figure 8: Effect of the center electrode area on the resonance and anti-resonance frequencies and their corresponding mechanical quality factors.

dramatically up to a = 0.4. This result is important, since fb and Q_B of non-electrode sample are used for calculating the extensive elastic compliance s_{11}^D, and mechanical loss tan . A non-electrode sample with up to 40% electrode area can give sufficiently accurate results for these values.

The Finite Element Method (FEM) analysis using FEM ATILA software [Version: ATILA ++ 3.0.27, and GID 12.0.9, Micro mechatronics, Inc., State College, PA] was conducted in [25], which were in good agreements with the experimental measurements. The FEM analysis is a practical tool for calculating the modes of vibrations, or strain and stress distributions for complex geometries. However, it is not an inexpensive software, nor easy one to use for electrical behavior characterization, in general [26,27]. We also reported a new six-terminal Mason's equivalent circuit (EC) model for non-electrode samples, by considering all three losses [26]. We demonstrated to obtain the voltage distribution in the non-electrode (NE) configuration with the equivalent circuit simulation. Each of the non-electrode load part was segmented into 20 elements along length. NE configuration elements behave under D-constant though the voltage could not be measured. The E-constant element was integrated in between the D-constant elements to measure the voltage distribution. The finite elements are connected in parallel as illustrated in (Figure 9). The maximum voltage occurs at the resonance frequency in this simulation. The results showed an improvement comparing with a conventional equivalent circuit with only one elastic loss parameter, and were generally in consistent with the experimental measurements. However, some mechanical quality parameters were calculated slightly lower than the experimental method [26]. It is essential to note that, for simplification, the EC considers discrete linear LCR components, while the FEM considers limited number of segmented parts for piezoelectric devices, resulting in approximated solutions for their behavior, which may be less accurate. Furthermore, the equivalent circuit method is still complicated from the viewpoint of the circuit design implementation in the required software.

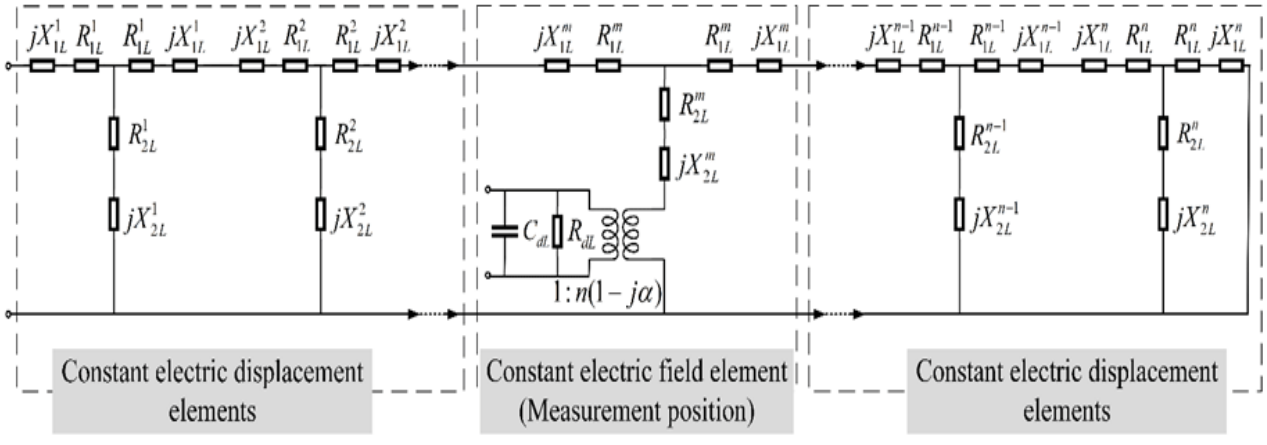

Figure 9: Finite element configuration of right (left) load to simulate the voltage distribution in NE configuration

The resonance frequencies and mechanical quality factors comparison for the analytical approach and experimental results, as well as the FEM ATILA simulation and EC method are summarized in (Table 3) for both FE sample and NE one with a = 0.1 (10%). The EC result was cited from [26], and was simulated with the proposed equivalent circuit by MATLAB [Version R2016a, The Math Works, Inc., Natick, Massachusetts]. On the other hand, the ATILA simulation results in this table were calculated from FEM ATILA simulation [Version: ATILA ++ 3.0.27, and GID 12.0.9, Micro mechatronics, Inc., State College, PA] and improved from [25] by integrating the material loss parameters with at least two digits of accuracy. As is shown, the analytical method gives the most accurate results, close to the experimental measurement values.

Finally, the voltage and strain distributions along the length versus the position x at a frequency where the maximum strain happens (mechanical resonance frequency) for the NE sample (a = 0.1) is demonstrated in (Figure 10) as an extension of the analytical solution, which has the same trend as FEM ATILA simulation results as in [25]. In FEM simulations, the maximum strain value is almost 1.3 times higher, and the maximum voltage value is 0.6 times lower than the analytical calculation.

Table 3: Comparison of the analytical solution with experimental results and other methods for FE and NE (with a = 0.1) samples

Samples	Experimental	FEM ATILA simulation	Equivalent Circuit	Analytical Solution
f_a – FE	40.69 ± 0.04	40.62	40.64	40.66
f_b – FE	42.31 ± 0.04	42.26	42.31	42.32
f_a – NE	42.43 ± 0.04	42.16	42.26	42.30
f_b – NE	42.85 ± 0.04	42.68	42.71	42.75
Q_A – FE	1390 ± 28	1390	1355	1390
Q_B – FE	1650 ± 33	1650	1567	1656
Q_A – NE	1690 ± 30	1629	1626	1648
Q_B – NE	1770 ± 35	1731	1708	1738

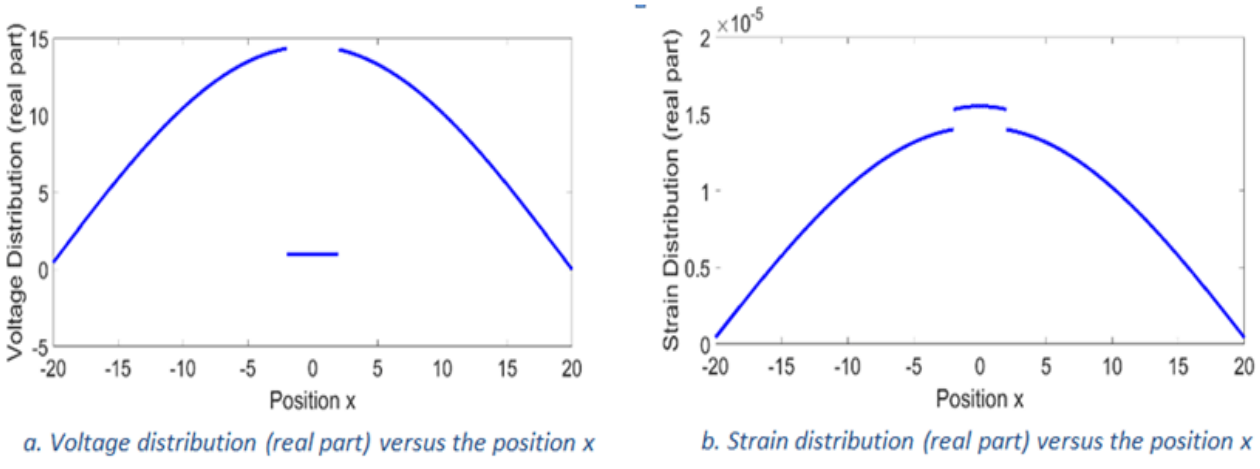

a. Voltage distribution (real part) versus the position x

b. Strain distribution (real part) versus the position x

Figure 10: Voltage and strain distributions along length for the NE sample (a = 0.1) – Analytical calculation.

Conclusion

In conclusion, this paper introduced an advanced piezoelectric characterization method with mechanical excitation on partial electrode samples, which can determine additional physical parameters the conventional IEEE Standard electrical excitation method cannot provide. In order to measure the side mechanical load, the admittance/impedance of the small center actuator part is monitored. First, an accurate analytical solution for deriving the resonance frequencies, mechanical quality factors and vibration mode in a partial non-electrode PZT rectangular plate in the k_{31} mode This was achieved by means of the dynamic and constitutive

equations, and solving the displacement and stress distributions with different boundary conditions for the electrode and non-electrode parts. This is important in the sense of calculating the extensive elastic compliance and mechanical loss, which can theoretically be measured from the mechanical excitation of a complete non-electrode sample. From the analytical solution, we found that a non-electrode sample with up to 40% electrode area can exhibit precise piezoelectric parameters including loss factors. Therefore, our experimental measurement calculations with neglecting the actuator part difference for the non-electrode sample with a = 10% in our previous paper [25] had almost accurate results. Those were in consistent with the "K" matrix indirect solution, and therefore, verify the validation of the indirect method, apart from its higher standard deviation.

Second, the new analytical method, compared with the FEM ATILA software and EC method, is more precise and also simple to use. This method can be further generalized for calculating the resonance frequencies and mechanical losses in complex structures with different boundary conditions and modes.

Acknowledgements

The authors acknowledge the support by funding from The Office of Naval Research (ONR) Grant Number: ONR N00014-17-1-2088.

References

1. Uchino K, Giniewicz JR. Micromechatronics. New York: Marcel Dekker. 2003.
2. Cagatay S, Koc B, Moses P, Uchino K. A piezoelectric Micromotor with a stator of φ= 1.6 mm and l= 4 mm using bulk PZT. Japanese Journal of Applied Physics. 2004;43(4A):1429-1433. doi: 10.1143/JJAP.43.1429
3. Paik DS, Yoo KH, Kang CY, Cho BH, Nam S, Yoon SJ. Multilayer piezoelectric linear ultrasonic motor for camera module. Journal of Electroceramics. 2009;22(1-3):346-351. doi: 10.1007/s10832-008-9513-3
4. Dembélé S, Rochdi K. A three DOF linear ultrasonic motor for transport and micropositioning. Sensors and Actuators A: Physical. 2006;125(2):486-493. doi: 10.1016/j.sna.2005.08.001
5. Priya S, Ural S, Kim HW, Uchino K, Ezaki T. Multilayered unipoled piezoelectric transformers. Japanese Journal of Applied Physics. 2004;43(6A):3503-3510. doi: 10.1143/JJAP.43.3503
6. Zhuang Y, Ural SO, Gosain R, Tuncdemir S, Amin A, Uchino K. High Power Piezoelectric Transformers with Pb (Mg1/3Nb2/3) O3–PbTiO3 Single Crystals. Applied Physics Express. 2009;2(12):121402. doi: 10.1143/APEX.2.121402
7. Wang F, Ge W, Yu P, Zhao X, Luo H, Zhang Y, et al. Multilayer Rosen-type piezoelectric transformer prepared with Pb (Mg1/3Nb2/3) O3–PbTiO3 single crystal. Journal of Physics D: Applied Physics. 2008;41(3):035409. doi: 10.1088/0022-3727/41/3/035409
8. Liu DKC, Friend J, Yeo L. A brief review of actuation at the micro-scale using electrostatics, electromagnetics and piezoelectric ultrasonics. Acoustical Science and Technology. 2010;31(2):115-123.
9. Watson B, Friend J, Yeo L. Piezoelectric ultrasonic micro/milli-scale actuators. Sensors and Actuators A: Physical. 2009;152(2): 219-233. doi: 10.1016/j.sna.2009.04.001
10. Uchino K. Ferroelectric Devices. New York: Marcel Dekker. 2008.
11. Tashiro S, Ikehiro M, Igarashi H. Influence of temperature rise and vibration level on electromechanical properties of high-power piezoelectric ceramics. Japanese Journal of Applied Physics. 1997;36(5B):3004-3009. doi: 10.1143/JJAP.36.3004
12. Hirose S, Aoyagi M, Tomikawa Y. Dielectric loss in a piezoelectric ceramic transducer under high-power operation; increase of dielectric loss and its influence on transducer efficiency. Japanese Journal of Applied Physics. 1993;32(5B):2418-2421. doi: 10.1143/JJAP.32.2418
13. Zhang S, Xia R, Lebrun L, Anderson D, Shrout TR. Piezoelectric materials for high power, high temperature applications. Materials Letters. 2005;59(27):3471-3475. doi: 10.1016/j.matlet.2005.06.016
14. UchinoK, Hirose S. Loss mechanisms in piezoelectrics: how to measure different losses separately. IEEE Trans. Sonics Ultrason. 2001;48(1):307-321. doi: 10.1109/58.896144
15. Holland R. Representation of dielectric, elastic, and piezoelectric losses by complex coefficients. IEEE Trans. Sonics Ultrason. 1967;14(1):18-20. doi: 10.1109/T-SU.1967.29405
16. Sherrit S, Wiederick HD, Mukherjee BK, Sayer M. An accurate equivalent circuit for the unloaded piezoelectric vibrator in the thickness mode. Journal of Physics D Applied Physics. 1999;30(16):2354-2363.
17. Uchino K, Zheng JH, Chen YH, Du XH, Ryu J, Gao Y, et al. Loss mechanisms and high power piezoelectrics. Journal of Materials Science. 2006;41(1):217-228. doi: 10.1007/s10853-005-7201-0
18. Callen HB. Thermodynamics and an Introduction to Themostatistics, 2nd ed. New York: John Wiley & Sons. 1985.
19. Lewis GN, Randall M. Thermodynamics. New York: McGraw-Hill Book Company. 1961.
20. Zhuang Y. The Pennsylvania State University, 2011. Available from: https://etda.libraries.psu.edu/files/final_submissions/6809
21. Zhuang Y, Ural SO, Tuncdemir S, Amin A, Uchino K. Analysis on loss anisotropy of piezoelectrics with∞ mm crystal symmetry. Jpn J Appl Phys. 2010;49(2R):021503-6. doi: 10.1143/JJAP.49.021503
22. Zhuang Y, Ural SO, Rajapurkar A, Tuncdemir S, Amin A, Uchino K. Derivation of piezoelectric losses from admittance spectra. Jpn J Appl Phys. 2009;48(4R):041401. doi: 10.1143/JJAP.48.041401
23. Shekhani HN, Gurdal EA, Ganapatibhotla L, Maranas JK, Staut R, Uchino K. The effect of electrical boundary conditions on the thermal properties of ferroelectric piezoelectric ceramics. arXiv preprint arXiv. 2016:1605.04836.
24. Lee SH, Yoon KH, Lee JK. Influence of electrode configurations on the quality factor and piezoelectric coupling constant of solidly mounted bulk acoustic wave resonators. J Appl Phys. 2002;92(7):4062-4069. doi: 10.1063/1.1505977

25. Majzoubi M, Shekhani HN, Bansal A, Hennig E, Scholehwar T, Uchino K. Advanced methodology for measuring the extensive elastic compliance and mechanical loss directly in k31 mode piezoelectric ceramic plates. J Appl Phys. 2016:120(22):225113-225117. doi: 10.1063/1.4971340
26. Dong X, Majzoubi M, Choi M, Ma Y, Hu M, Jin L, et al. A new equivalent circuit for piezoelectrics with three losses and external loads. Sensors and Actuators A: Physical. 2017;256(1):77-83.
27. Al-Budairi H, Lucas M, Harkness P. A design approach for longitudinal–torsional ultrasonic transducers. Sensors and Actuators A: Physical. 2013;198(15):99-106. doi: 10.1016/j.sna.2013.04.024
28. ANSI/IEEE 176-1987 (1987), IEEE Standard on Piezoelectricity. New York: The Institute of Electrical and Electronics Engineers.
29. Daneshpajooh H, Shekhani HN, Choi M, Uchino K. New methodology for determining the dielectric constant of a piezoelectric material at the resonance frequency range. J Am Ceram Soc. 2017. doi: 10.1111/jace.15338